International Journal of Solids and Structures 48 (2011) 1696–1710

Contents lists available at ScienceDirect

International Journal of Solids and Structures

journal homepage: www.elsevier.com/locate/ijsolstr

Void growth and coalescence in anisotropic plastic solids

S.M. Keralavarma *, S. Hoelscher, A.A. Benzerga

Department of Aerospace Engineering, Texas A&M University, College Station, TX 77843-3141, USA

ARTICLE INFO

Article history:
Received 16 May 2010
Received in revised form 16 February 2011
Available online 26 February 2011

Keywords:
A. Ductile fracture
A. Voids and inclusions
B. Finite element analysis
B. Porous metal plasticity
C. Anisotropy
C. Constitutive behavior

ABSTRACT

Large strain finite element calculations of unit cells subjected to triaxial axisymmetric loadings are presented for plastically orthotropic materials containing a periodic distribution of aligned spheroidal voids. The spatial distribution of voids and the plastic flow properties of the matrix are assumed to respect transverse isotropy about the axis of symmetry of the imposed loading so that a two-dimensional axisymmetric analysis is adequate. The parameters varied pertain to load triaxiality, matrix anisotropy, initial porosity and initial void shape so as to include the limiting case of penny-shaped cracks. Attention is focussed on comparing the individual and coupled effects of void shape and material anisotropy on the effective stress–strain response and on the evolution of microstructural variables. In addition, the effect of matrix anisotropy on the mode of plastic flow localization is discussed. From the results, two distinct regimes of behavior are identified: (i) at high triaxialities, the effect of material anisotropy is found to be persistent, unlike that of initial void shape and (ii) at moderate triaxialities the influence of void shape is found to depend strongly on matrix anisotropy. The findings are interpreted in light of recent, microscopically informed models of porous metal plasticity. Conversely, observations are made in relation to the relevance of these results in the development and calibration of a broader set of continuum damage mechanics models.

1. Introduction

Ductile fracture in structural materials results from the nucleation, growth and coalescence of micro-voids that initiate from second phase particles and inclusions. Accurate modeling of void growth and coalescence under arbitrary imposed loading conditions is critical to the predictive modeling of ductile fracture. Gurson (1977) derived an analytical model of void growth in an *isotropic* medium based on analysis of a spherical representative volume element (RVE) made of an ideal plastic von Mises material and containing a concentric spherical void. The somewhat idealized choice of the RVE geometry was dictated by the complexity of the analytical approach. Alternatively, finite element (FE) calculations of appropriately chosen unit cells subjected to a remote triaxial loading have been used to simulate periodic arrays of voids. Needleman (1972) performed a two-dimensional plane-strain analysis of a periodic array of cylindrical voids in an isotropic matrix, while a transverse isotropic distribution of spherical voids in an isotropic matrix was analyzed by Tvergaard (1982) and later by Koplik and Needleman (1988). The finite element results were used as benchmarks to calibrate the Gurson model and heuristic corrections were suggested to enhance the quantitative agreement between the model and the cell calculations (Tvergaard, 1982; Tvergaard and Needleman, 1984). Subsequently, three-dimensional investigations of cubic patterns of spherical voids (Hom and McMeeking, 1989; Worswick and Pick, 1990) under triaxial loadings have evidenced good agreement with the axisymmetric calculations. In particular, these unit cell computations identified the porosity and the loading triaxiality (the ratio of the mean to the von Mises effective stress) as key parameters affecting void growth and coalescence. More recent unit cell analyses of initially spherical voids have also shown some influence of the third invariant of the stress tensor, through the Lode parameter, on void growth and coalescence (Benzerga and Besson, 2001; Zhang et al., 2001; Kim et al., 2004; Gao and Kim, 2006; Barsoum and Faleskog, 2007). FE Cell model studies have *de facto* become a major tool in understanding material behavior at intermediate scales and were recently reviewed by Benzerga and Leblond (2010), including aspects pertaining to the void nucleation stage.

In recent years, various extensions of the Gurson model have been proposed which account for initial or deformation-induced anisotropies (Gologanu et al., 1993, 1997; Benzerga and Besson, 2001; Monchiet et al., 2008; Keralavarma and Benzerga, 2008, 2010). The commonality among these models is that they are based on micromechanical treatments, with homogenization and limit analysis being the theoretical foundation (Benzerga and Leblond, 2010). The performance of the model of Gologanu et al. (1997) in predicting void shape effects has been assessed by Sovik and Thaulow (1997), and more thoroughly by Pardoen and

* Corresponding author.
E-mail address: skeralavarma@tamu.edu (S.M. Keralavarma).

0020-7683/$ - see front matter © 2011 Elsevier Ltd. All rights reserved.
doi:10.1016/j.ijsolstr.2011.02.020

Hutchinson (2000), who used the unit cell model considering initially spheroidal voids in an isotropic matrix. Similarly, Benzerga and Besson (2001) carried out a series of unit cell calculations for initially spherical voids embedded in a transversely isotropic matrix. They have shown that their extension of the Gurson model to orthotropic matrices provided a good quantitative prediction of the voided cell results for sufficiently high stress triaxialities.

However, the more general models that combine effects of void shape and plastic anisotropy have not yet been assessed against the voided cell model. Keralavarma and Benzerga (2010) presented some preliminary results to motivate their development of a new porous metal plasticity model. Also, their set of calculations focussed on pre-localization void growth. The objective of this paper is to report on a large set of such calculations, probing the parameter space much beyond the report of Keralavarma and Benzerga (2010). While we offer new findings by means of the voided cell model, the present results can also serve as reference to calibrate advanced models of ductile fracture. General conditions of transverse isotropy are discussed and used, thus enabling a two-dimensional axisymmetric analysis. Emphasis is laid on the combined effects of void shape and matrix anisotropy on void growth and micro-scale flow localization, the latter setting the stage for void coalescence.

2. Problem formulation

The void distribution in the plane of transverse isotropy of the matrix is an approximation of a hexagonal arrangement. Such a microstructure may be constructed from an infinite repetition of the unit cell sketched in Fig. 1a. The hatched bands in the figure schematically represent the texture of the matrix. Fig. 1b shows a planar cross section of the unit cell in Fig. 1a. A cylindrical unit cell is taken to approximate this hexagonal arrangement and is sketched in Fig. 1c (front view) and Fig. 1d (top view). The boundaries of the unit cell are constrained to remain straight from considerations of periodicity, in the absence of shear loading, so that the RVE retains its cylindrical shape during deformation. Exploiting the symmetry of the problem, one only needs to mesh the shaded region in Fig. 1b. Let $(\mathbf{e}_L, \mathbf{e}_T, \mathbf{e}_S)$ denote the triad associated with the orthotropy of the matrix (Fig. 1c). We also define a Cartesian coordinate system $(\mathbf{e}_1, \mathbf{e}_2, \mathbf{e}_3)$ as shown in Fig. 1d where $\mathbf{e}_3$ is aligned

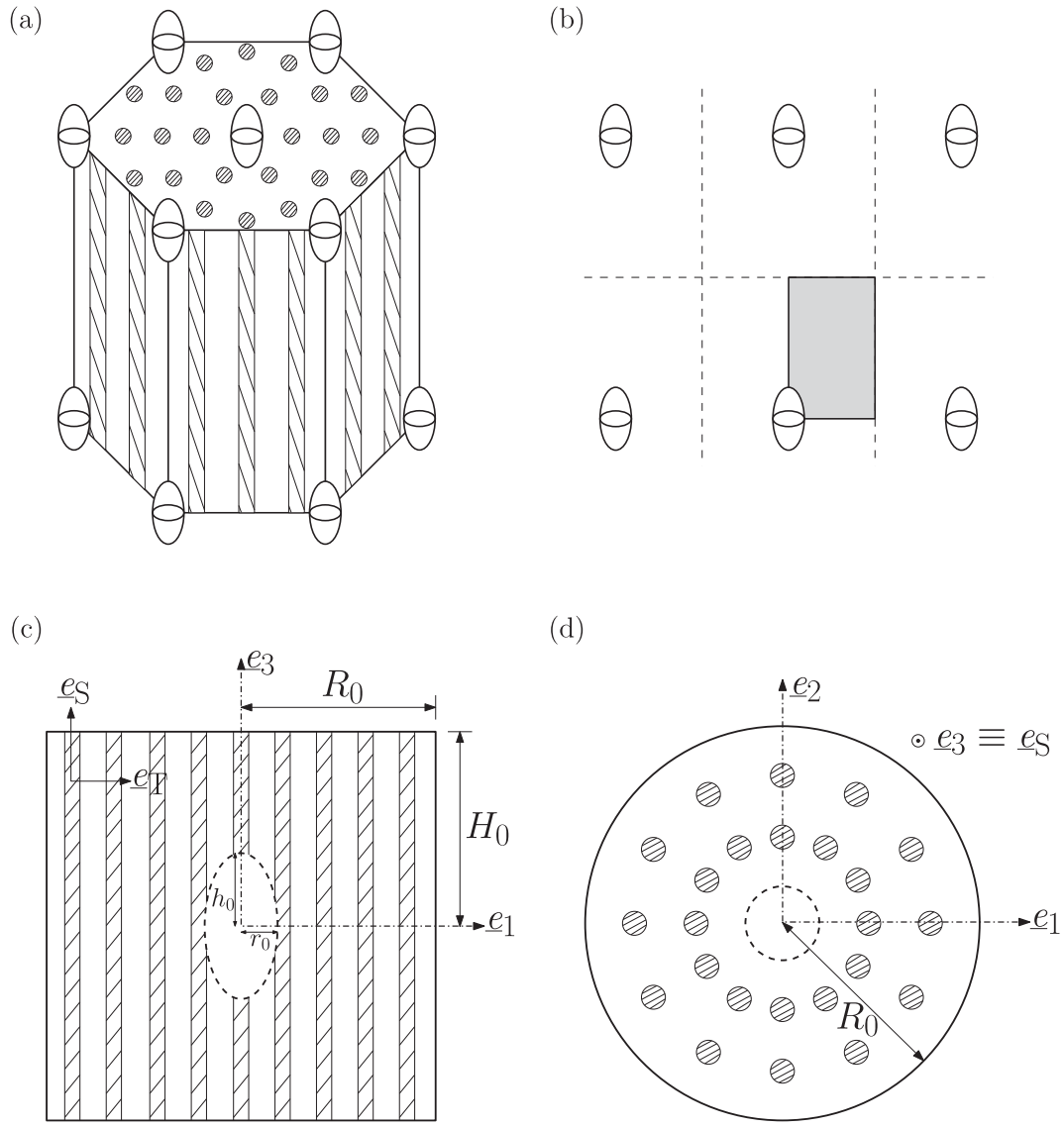

Fig. 1. Idealized representation of the microstructure in the voided cell model: (a) hexagonal periodic unit and (b) cross-section in the plane of the paper. Cylindrical unit cell used in the axisymmetric calculations: (c) front view and (d) top view.

with the common axis of the voids. The latter is itself identified with the axis of transverse isotropy of the matrix, i.e. $\mathbf{e}_3 \equiv \mathbf{e}_S$, so that the effective behavior of the unit cell is transversely isotropic, and one may perform axisymmetric calculations.

Our finite element implementation of the voided cell model follows that of Benzerga and Besson (2001) using the object oriented code ZeBuLoN (Besson and Foerch, 1997). The weak form of the momentum balance for a body undergoing finite deformations in the absence of body forces is generally written as

$$\int_V \mathbf{S} : \delta\mathbf{E}\, dV = \int_S \mathbf{T} \cdot \delta\mathbf{u}\, dS \tag{1}$$

with

$$\mathbf{S} = J\mathbf{F}^{-1} \cdot \boldsymbol{\sigma} \cdot \mathbf{F}^{-T}, \quad \mathbf{E} = \frac{1}{2}(\mathbf{F}^T \cdot \mathbf{F} - \mathbf{I}), \tag{2}$$

where $\mathbf{S}$ is the symmetric second Piola–Kirchoff stress tensor, $\mathbf{E}$ is the Green–Lagrange strain, $\mathbf{F}$ is the deformation gradient, $J = \det(\mathbf{F})$, $\mathbf{I}$ is the second-order identity tensor, $\boldsymbol{\sigma}$ is the Cauchy stress, $\mathbf{T}$ is the surface traction in the reference configuration, $\mathbf{u}$ is the displacement vector and V and S are respectively the volume and surface of the body in the reference configuration. An updated Lagrangian formulation is used (Ladeveze, 1980; Hughes and Winget, 1980) which employs objective space frames with the reference configuration being chosen at the end of the increment so that the stress measure $\mathbf{S}$ reduces to the Cauchy stress.

The material constitutive model is assumed to be that of a rate-independent elastically isotropic and plastically anisotropic solid. In the objective frame, the deformation rate tensor is written as the sum of an elastic part, $\mathbf{d}^e$, and a plastic part, $\mathbf{d}^p$. Assuming small elastic strains and isotropic elasticity, a hypo-elastic law is expressed in terms of the rotated stress $\mathbf{P}$

$$\mathbf{d}^e = \mathbb{C}^{-1} : \dot{\mathbf{P}}, \quad \mathbf{P} = J\mathbf{R}^T \cdot \boldsymbol{\sigma} \cdot \mathbf{R}, \tag{3}$$

where $\mathbb{C}$ is the rotated tensor of elastic modulii and $\mathbf{R}$ is the skew-symmetric tensor obtained from the polar decomposition of the deformation gradient, so that the Green–Naghdi rate of $\boldsymbol{\sigma}$ is used. The plastic part of the deformation rate $\mathbf{d}^p$ is obtained by normality from an orthotropic yield function of the Hill (1948) type, $\mathcal{F}(\boldsymbol{\sigma})$.

$$\mathbf{d}^p = \Lambda \frac{\partial \mathcal{F}}{\partial \boldsymbol{\sigma}}, \quad \mathcal{F}(\boldsymbol{\sigma}) = \frac{3}{2}\boldsymbol{\sigma} : \mathbb{p} : \boldsymbol{\sigma} - \bar{\sigma} = \frac{3}{2}\boldsymbol{\sigma}' : \mathbb{h} : \boldsymbol{\sigma}' - \bar{\sigma}, \tag{4}$$

where Λ is the plastic multiplier, $\boldsymbol{\sigma}' = \boldsymbol{\sigma} - \frac{1}{3}\mathrm{tr}(\boldsymbol{\sigma})\mathbf{I}$ is the stress deviator, $\mathbb{p}$ is the Hill (1948) anisotropy tensor, $\mathbb{h}$ is the anisotropy tensor in the space of deviatoric stresses (related to $\mathbb{p}$ through $\mathbb{p} = \mathbb{J} : \mathbb{h} : \mathbb{J}$ where $\mathbb{J} = \mathbb{I} - \frac{1}{3}\mathbf{I} \otimes \mathbf{I}$ is the deviatoric projector, $\mathbf{I}$ being the 4th order identity tensor; see (Benzerga and Besson, 2001)). Also, $\bar{\sigma}$ is the flow stress in an arbitrarily chosen reference direction. An isotropic power law hardening model is assumed, of the form

$$\bar{\sigma}(p) = \sigma_S\left(\frac{p}{\epsilon_0} + 1\right)^n, \quad \epsilon_0 = \frac{\sigma_S}{E}, \tag{5}$$

where p is an effective measure of plastic strain defined to be work conjugate to $\bar{\sigma}$. p is obtained through $p = \int_0^t \dot{p}dt$ with

$$\dot{p} = \sqrt{\frac{2}{3}\mathbf{d}^p : \hat{\mathbb{p}} : \mathbf{d}^p}, \tag{6}$$

where $\hat{\mathbb{p}}$ is a formal inverse of Hill's tensor $\mathbb{p}$ defined through $\mathbb{p} : \hat{\mathbb{p}} = \hat{\mathbb{p}} : \mathbb{p} = \mathbb{J}$. In (5) σ_S is the initial matrix yield stress in the axial direction $\mathbf{e}_S$, n is the hardening exponent and E is Young's modulus. A fully implicit time integration procedure was used, based on an iterative Newton–Raphson method, and the consistent tangent matrix was obtained following Simo and Taylor (1985).

Traction-free boundary conditions are imposed on the surface of the void while symmetry conditions are imposed on the bottom and left boundaries of the cell quadrant (Fig. 1b). Special boundary conditions are formulated whereby the displacement of the top surface is incremented at a constant rate while the displacements of the lateral boundary are iteratively adjusted to maintain a constant stress triaxiality ratio at every step of the deformation. The principal components of the macroscopic stress tensor, $\boldsymbol{\Sigma}$, are obtained by integrating the surface tractions along the external cell boundary such that

$$\Sigma_{11} = \Sigma_{22} = \frac{R_0}{RH}\int_0^{H_0} [T_1]_{X_1^2+X_2^2=R_0^2} dX_3, \quad \Sigma_{33} = \frac{2}{R^2}\int_0^{R_0} [T_3]_{X_3=H_0} X_1 dX_1, \tag{7}$$

where X_i are the components of the position vector $\mathbf{X}$ in the initial configuration, R and H are respectively the radius and half the height of the unit cell in the current configuration and R_0 and H_0 are the corresponding quantities in the initial configuration (see Fig. 1c). The principal components of the macroscopic strain tensor, $\mathbf{E}$, for the unit cell are written as

$$E_{11} = E_{22} = \log\frac{R}{R_0}, \quad E_{33} = \log\frac{H}{H_0}. \tag{8}$$

We consider remote axisymmetric loadings of the type $\boldsymbol{\Sigma} = \Sigma_{11}(\mathbf{e}_1 \otimes \mathbf{e}_1 + \mathbf{e}_2 \otimes \mathbf{e}_2) + \Sigma_{33}\mathbf{e}_3 \otimes \mathbf{e}_3$. The stress triaxiality ratio, T, is related to the ratio of radial to axial stresses, θ, through

$$T \equiv \frac{\Sigma_m}{\Sigma_e} = \frac{1}{3}\frac{2\theta + 1}{|1 - \theta|}, \quad \theta \equiv \frac{\Sigma_{11}}{\Sigma_{33}}, \tag{9}$$

where Σ_m and Σ_e denote the mean and von Mises effective macroscopic stresses, respectively given by

$$\Sigma_m = \frac{1}{3}\mathrm{tr}(\boldsymbol{\Sigma}) = \frac{2\Sigma_{11} + \Sigma_{33}}{3}, \quad \Sigma_e = \sqrt{\frac{3}{2}\boldsymbol{\Sigma}' : \boldsymbol{\Sigma}'} = |\Sigma_{33} - \Sigma_{11}|. \tag{10}$$

Each value of T is generally associated with two distinct values of θ corresponding to a major axial stress ($\theta < 1$) and a major radial stress ($\theta > 1$). In this study we restrict our attention to cases of major axial stress ($\theta < 1$). Each calculation is carried out under conditions of a constant imposed triaxiality (proportional loading path). We investigate the material response under moderate ($T = 1$) to high ($T = 2,3$) values of the stress triaxiality as are prevalent in notched bars or in the plastic zone ahead of a blunted crack tip. An effective strain measure work conjugate to Σ_e is given by

$$E_e = \frac{2}{3}|E_{33} - E_{11}|. \tag{11}$$

The effective stress and strain measures defined above are used to compare the stress–strain responses of the unit cells in all the results presented here.

In the frame of material orthotropy, the anisotropy tensor $\mathbb{h}$ in (4) is represented thanks to Voigt's reduction by a diagonal 6×6 matrix whose diagonal elements, designated h_L, h_T, h_S, h_{TS}, h_{SL}, h_{LT}, completely characterize the orthotropy of the matrix. An extensive tabulation of the available experimental data on the Hill coefficients of structural metals was provided by Benzerga (2000). Here, we restrict our attention to transversely isotropic materials subjected to axisymmetric loading aligned with the axis of material symmetry, taken to be $\mathbf{e}_S$. The requirement of transverse isotropy about $\mathbf{e}_S$ further entails that $h_L = h_T = h_{LT}$ and $h_{TS} = h_{SL}$ since the directions $\mathbf{e}_L$ and $\mathbf{e}_T$ are equivalent.

In this paper we investigate five different material categories, including the isotropic case, Table 1. The Hill coefficients in Table 1 are chosen to span the experimental ranges of values tabulated in (Benzerga, 2000) (see Annexe-A-V). Materials (ib) and (iib) are variants of material categories (i) and (ii) previously employed by Benzerga and Besson (2001) with lower values of the out-of-plane "shear" Hill coefficients $h_{TS} = h_{SL}$. Material categories (i)

Table 1
The five matrix material categories and corresponding anisotropy parameters used in the unit cell calculations. Coefficients h_i (i = L,T,S,TS,SL,LT) represent the diagonal elements of the Voigt representation of anisotropy tensor $\mathbb{h}$, expressed in the frame of material orthotropy, and h is a scalar invariant of $\mathbb{h}$ defined in Eq. (14). Wider ranges of variation of h_{TS} were also reported in the literature.

	h_L	h_T	h_S	h_{TS}	h_{SL}	h_{LT}	Notes		h
Isotropic	1.000	1.000	1.000	1.000	1.000	1.000	Reference	EYT	2.000
Material (ib)	1.000	1.000	1.000	2.333	2.333	1.000	Weak in shear	EYT	1.757
Material (iib)	0.667	0.667	1.167	1.750	1.750	0.667	Weak in shear	S-soft	2.028
Material (iii)	1.000	1.000	1.000	0.500	0.500	1.000	Shear resistant	EYT	2.366
Material (iv)	2.333	2.333	0.333	1.000	1.000	2.333	Shear resistant	S-hard	1.757

and (ii) have relatively high values of the shear Hill coefficients $h_{TS}(=h_{SL})$ compared to the isotropic case making them weaker under shear than under tensile loading in the principal directions. The opposite is true for material categories (iii) and (iv). In addition, materials (ib) and (iii) have equal yield strengths in tension (EYT) along the principal directions. This is not the case for the other materials, which are assumed to have the same yield stresses as the isotropic material along $\mathbf{e}_L$ and $\mathbf{e}_T$ while being softer (material (iib)) or harder (material (iv)) in tension along $\mathbf{e}_S$. Material categories (ii) and (iv) are closer to realistic material parameters as tabulated by Benzerga (2000). However, categories (i) and (iii) were chosen for ease of interpretation of the results, as will be shown below. In another set of calculations, the coefficient $h_{TS}(=h_{SL})$ is systematically varied in the case of material category (iii).

Besides the Hill anisotropy factors for the matrix, the microstructure in the cell model is completely specified by three dimensionless parameters: the void volume fraction, f, the void aspect ratio, w, representing the average void shape and the cell aspect ratio, λ, representing the anisotropy in void distribution. These are defined by

$$f = 1 - (1 - f_0)\frac{R_0^2 H_0}{R^2 H}\left(1 + \frac{3(1-2\nu)}{E}\Sigma_m\right), \quad w = \frac{h}{r}, \quad \lambda = \frac{H}{R}, \tag{12}$$

where f_0 denotes the initial porosity, ν is the Poisson's ratio and r and h respectively denote the radial and axial semi-axes of the void in the current configuration (Fig. 1c). The expression for f is obtained using the plastic incompressibility condition for the matrix and the approximation of Koplik and Needleman (1988) for the elastic dilation. The ranges of all the parameters being explored in this study are tabulated in Table 2. Unlike the Hill coefficients, the values of these microstructural variables evolve during deformation. A subscript 0 is used in the remainder of this paper to indicate values in the undeformed configuration. The case $w_0 = 1/30$ corresponds to a penny-shaped crack and other values of 1/10 and 1/20 were used in probing limit behavior. The value of the strain hardening exponent n is taken to be 0.1 in all calculations.

Typical meshes employed in this study are shown in Fig. 2. Since the meshes undergo significant elongation in the axial direction due to the influence of the major axial stress, initially flat elements are used in the expected necking zone (the ligament separating the voids in the radial direction) using appropriate grading of the edge nodes. In most calculations void coalescence took place by strain localization along the radial ligament, for which meshes of the type shown in Fig. 2 were used. However, certain types of material anisotropy were observed to promote strain localization away from the radial direction. For materials that exhibited this trend, we have used alternate (finer) meshes with a uniform element density throughout the domain so as to capture better the details of the localization band.

Table 2
Ranges of initial microstructural and loading parameters considered in the unit cell calculations.

Parameter	Values used
f_0	0.0001, 0.001
w_0	1/30*, 1/6, 1/2, 1, 2, 6
λ_0	1
T	1, 2, 3

* Requires special choice of porosity as discussed in Section 3.4.

3. Results

3.1. Basic phenomenology

The deformation of the unit cell under axisymmetric loading exhibits two distinct stages: (i) void growth aided by diffuse plastic deformation in the matrix and (ii) void growth through localization of plastic deformation in the inter-void ligament, leading to void coalescence. These stages are illustrated in Fig. 3. The transition between them, which is indicated with the $\times$ mark, is referred to as the *onset* of void coalescence. The latter is a continuous process occurring over a narrow strain window but rather large windows of stress and porosity. Fig. 3a shows the effective stress–strain response for a unit cell containing an initially spherical void in an isotropic matrix, subjected to a stress triaxiality ratio $T = 2$. Here, and in all subsequent stress–strain plots, the effective stress is normalized by σ_S; see Eq. (5). The onset of coalescence is accompanied by a rapid drop in the stress carrying capacity of the unit cell. As discussed by Koplik and Needleman (1988), the transition from the void growth to the coalescence stage may be discerned by a transition from a triaxial to a uniaxial mode of deformation for the cell, i.e. the cell deforms uniaxially in the $\mathbf{e}_3$ direction while plasticity localizes to the intervoid ligament along the radial direction. This behavior is clearly seen in Fig. 3d. The stage of micro-scale localization (past the $\times$ mark) is also accompanied by an accelerated growth of porosity (Fig. 3b) and a rapid drop in the void aspect ratio (Fig. 3c) due to the lateral void expansion during ligament necking. The void volume fraction (or porosity f) is accurately estimated from the overall volumetric expansion of the cell using the plastic incompressibility property of the matrix. However, the void aspect ratio w, as defined in (12) and shown in Fig. 3c and subsequent figures, describes the actual void shape only approximately. Under certain circumstances, such as in the post-localization stage, the void shape may substantially deviate from a spheroid so that w alone no longer characterizes the true void shape accurately.

In what follows, the effective strain to coalescence, $E^{(c)}$, and the void volume fraction at the onset of coalescence, $f^{(c)}$, are defined as the values taken by E_e and f at the onset of micro-scale localization. These measures will be used to compare the various cases as we explore the parameter space.

3.2. Regime of high triaxiality

We first consider the high triaxiality case due to its importance in crack growth studies. The stress triaxiality prevailing in the

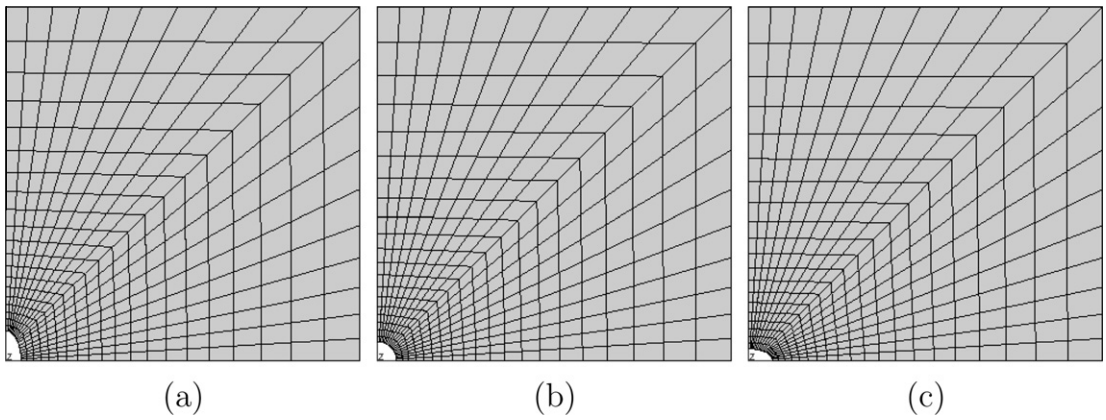

Fig. 2. FE meshes used in some calculations corresponding to $f_0 = 0.0001$, $\lambda_0 = 1$ and (a) $w_0 = 2$, (b) $w_0 = 1$, (c) $w_0 = 1/2$.

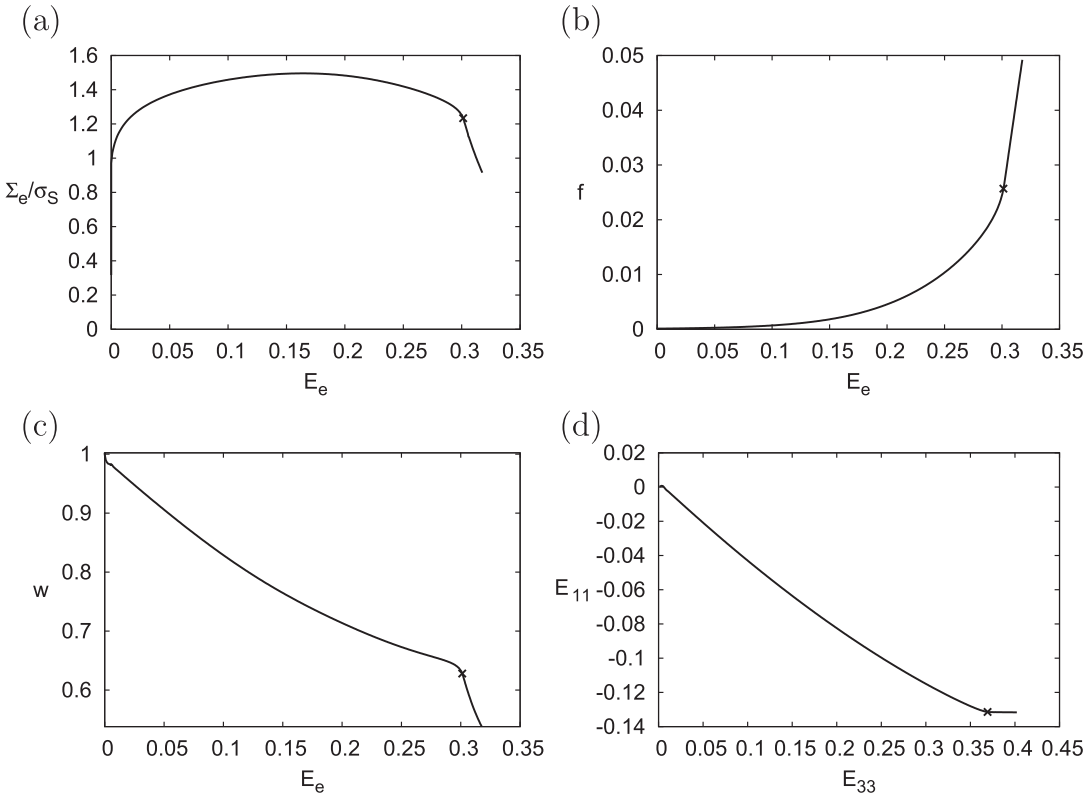

Fig. 3. A typical emergent behavior in a cell model calculation for an initially spherical void in an isotropic matrix using $f_0 = 0.0001$, $\lambda_0 = 1$ and $T = 2$. (a) Effective stress–strain response. (b) Evolution of porosity. (c) Evolution of void aspect ratio. (d) Radial strain E_{11} versus axial strain E_{33}. The $\times$ mark on each curve indicates the onset of coalescence.

crack tip plastic zones of thick specimens is typically in the range 2–3. A highly triaxial stress state significantly enhances void growth since the rate of porosity growth has a well known exponential dependence on the mean normal stress prior to localization. Fig. 4 shows results for $T = 2$ and three EYT matrix materials: isotropic, material (ib) and material (iii) from Table 1. EYT materials have equal yield stresses in the three principal directions of orthotropy, and this leads to roughly similar values for the effective yield stresses (see Fig. 4a). This is desirable in drawing comparisons, since the porosity rate has an exponential dependence on the mean stress. In particular, any differences in the porosity rates between the three materials (at least in the initial hardening regime) would result from differences in void shapes and Hill anisotropy parameters and not from the different stress levels. Materials (ib) and (iii) are differentiated only by the values of the "shear" Hill coefficients $h_{TS} = h_{SL}$ with material (ib) having a lower yield stress under shear in the T-S plane than the isotropic material and material (iii) having a higher shear yield stress than the isotropic material. For each material, three different initial void shapes, $w_0 = 2$ (prolate), $w_0 = 1$ (spherical) and $w_0 = 1/2$ (oblate) are compared. The stress–strain response of the dense matrix ($f \equiv 0$) is also shown as a reference. All calculations were continued beyond the onset of coalescence (Fig. 4d).

The results in Fig. 4 clearly indicate a strong effect of matrix material anisotropy on void growth and coalescence thus affecting the gradual loss of stress bearing capacity of the porous material.

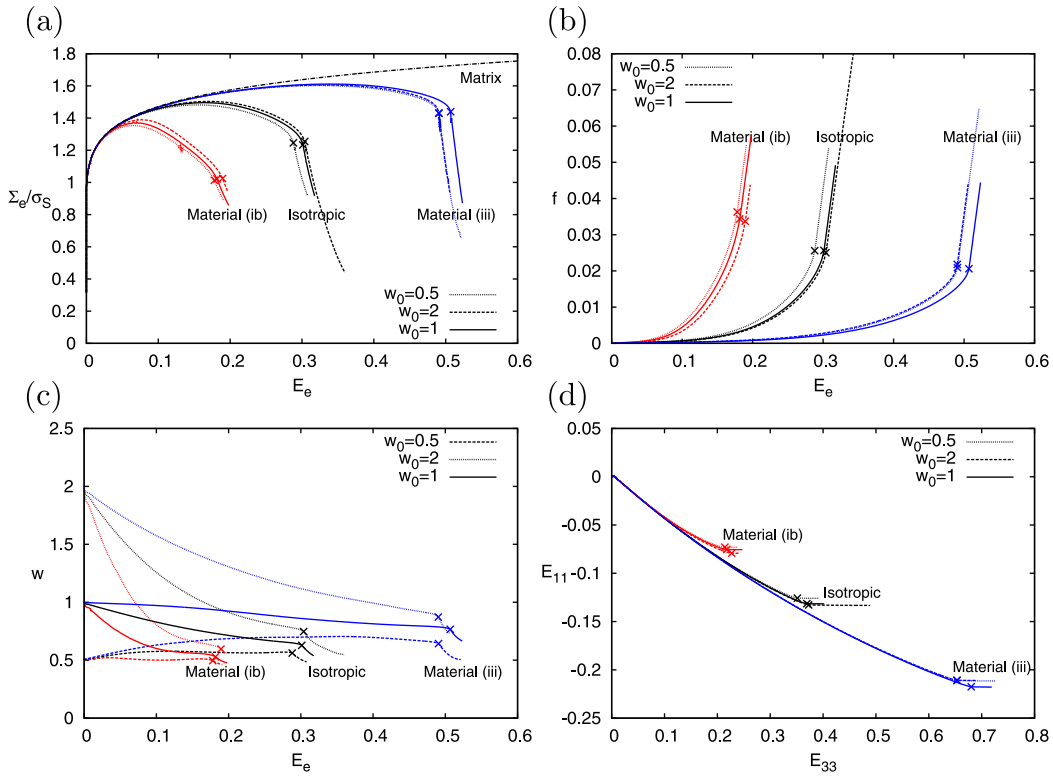

Fig. 4. Effect of matrix material anisotropy on the cell model response for $f_0 = 0.0001$, $\lambda_0 = 1$, $T = 2$ and three values of w_0. Case of EYT (equal yield in tension) materials (Table 1). (a) Effective stress–strain response, (b) evolution of porosity, (c) evolution of the void aspect ratio and (d) radial strain E_{11} vs. axial strain E_{33}.

On the other hand, the initial void shape has a minor effect at the triaxiality level considered here. Further, unit cells made of material (ib) are seen to have the highest rates of void growth and lowest ductility (Fig. 4b) along with an accelerated void growth in the lateral direction (note the faster drop in w with increasing E_e in Fig. 4c). On the other hand, material (iii) exhibits the slowest rate of void growth and the highest ductility.

Similar trends are shown in Fig. 5 for a loading triaxiality $T = 3$ with the effect of void shape becoming even less noticeable, especially for materials (ib) and the isotropic matrix. Notice that the effective strain to coalescence is much lower at $T = 3$ as compared to $T = 2$ for each material, due to the accelerated void growth resulting from the higher mean normal stresses. Fig. 6a-c show the contours of the matrix effective plastic strain, p, for the three materials at the same unit cell effective strain. Material (ib) shows the maximum void enlargement, consistent with the results in Fig. 5b. Note that the voids develop into oblate shapes although the major load is axial. This typically nonlinear effect is visible for the isotropic material and is more clear for material (ib). In fact the void configuration in the case of material (ib) is very close to the critical configuration for the onset of coalescence while material (iii) shows the least void growth. Finally, we note that in all the calculations at high T ($T \geqslant 2$) coalescence occurred by necking of the inter-void ligament in the radial direction.

Fig. 7 summarizes our results for EYT materials in the range of triaxiality $T = 1$ to $T = 3$ and for an initial porosity $f_0 = 0.0001$. Fig. 7a shows the effective strain to coalescence, $E^{(c)}$, for initially spherical voids as a function of the loading triaxiality. Material (iii) systematically exhibits higher coalescence strains as compared to an isotropic material while material (ib) exhibits lower ductility

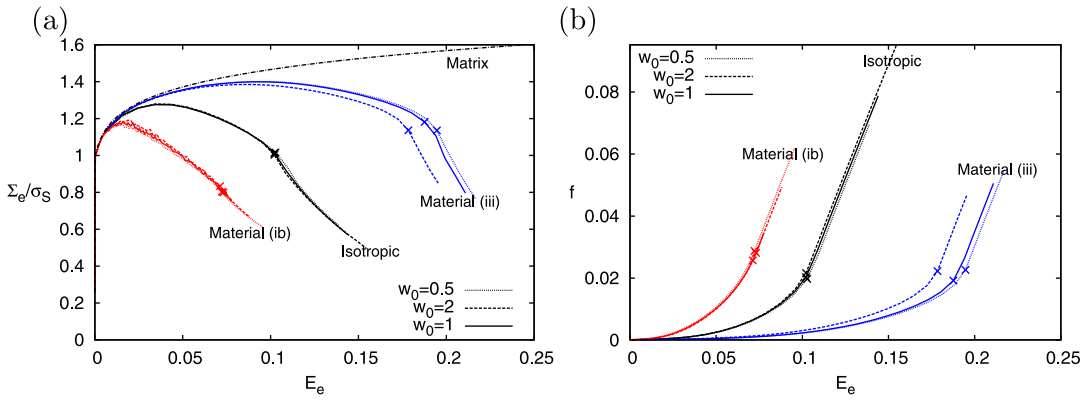

Fig. 5. Effect of matrix material anisotropy on the cell model response for $f_0 = 0.0001$, $\lambda_0 = 1$, $T = 3$ and three values of w_0. Case of EYT (equal yield in tension) materials (Table 1). (a) Effective stress–strain response, and (b) evolution of porosity.

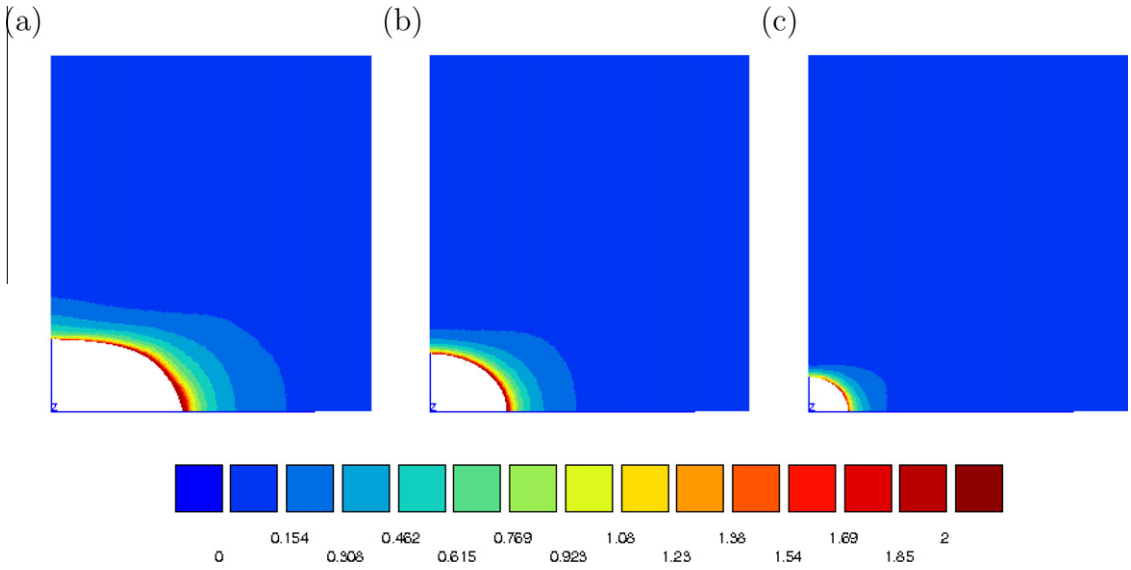

Fig. 6. Contours of effective plastic strain p in the current configuration at a unit cell effective strain $E_e = 0.07$ for initially spherical voids with $f_0 = 0.0001$, $\lambda_0 = 1$ and $T = 3$: (a) material (ib), (b) isotropic material, and (c) material (iii).

than the isotropic material for all values of T considered. While there is an apparent reduction in the ductility difference between the three materials at higher triaxialities, the relative differences are nevertheless significant, as already shown in Figs. 4 and 5.

To quantify the effect of the initial void shape for a given matrix material, we define an *ad hoc* void shape sensitivity parameter, $\Delta E^{(c)}$, by

$$\Delta E^{(c)} \equiv E^{(c)}_{w_0=2} - E^{(c)}_{w_0=1/2}, \tag{13}$$

i.e. the difference in the void coalescence strains between the initially prolate and oblate voids with aspect ratios 2 and 1/2 respectively. Fig. 7b shows the variation of $\Delta E^{(c)}$ as a function of T for each EYT material considered. In all cases, $\Delta E^{(c)}$ approaches zero at $T \geqslant 2$ indicating a reduced sensitivity for the ductility to the initial void shape at high triaxialities. On the other hand, at $T = 1$, the isotropic material and material (ib) show a high sensitivity to the initial void shape while material (iii) shows a low void shape sensitivity.

One conclusion that already emerges from this work is that while the effect of void shape vanishes at high stress triaxiality, that of material anisotropy persists. Another emergent behavior is that certain forms of matrix material anisotropy (namely shear-resistant materials of category (iii)) seem to render the effect of void shape less relevant, even at moderate triaxiality. This indicates a strong coupling between void shape effects and material anisotropy. This issue is examined in greater detail in the following section.

3.3. Regime of moderate triaxiality

The effect of void shape on the unit cell response at $T = 1$ and in the case of an isotropic matrix is illustrated in Fig. 8. In this section, $\lambda_0 = 1$ as above and, unless otherwise noted, the initial porosity is $f_0 = 0.001$. Unlike at high triaxialities, the initial void shape has a clear effect on both the evolution of porosity and the strains to coalescence. This is in keeping with the trends seen in previous investigations focused on isotropic materials (Pardoen and Hutchinson, 2000).

At the same moderate triaxiality ($T = 1$), the effect of matrix material anisotropy is illustrated in Fig. 9 for initially spherical voids. As above, focus is restricted to EYT materials, Table 1. The

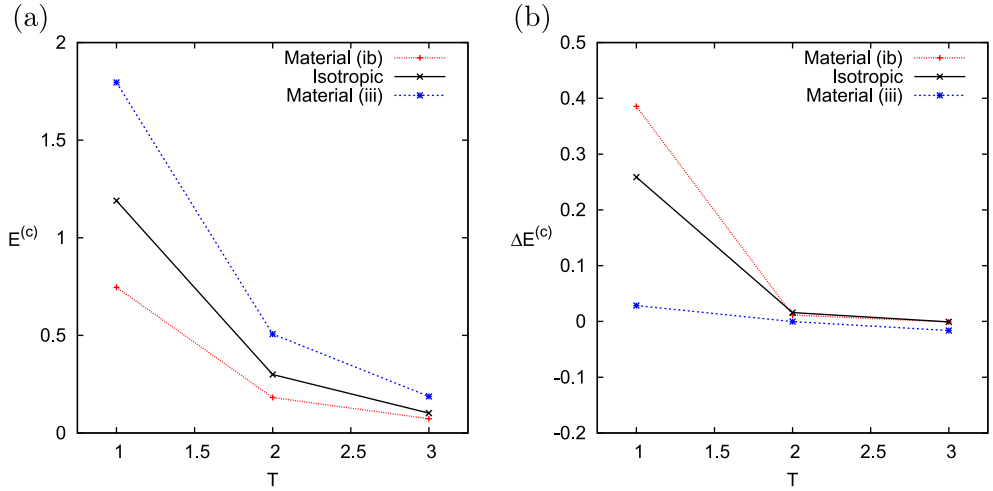

Fig. 7. Variation of (a) the effective strain to coalescence, $E^{(c)}$, for spherical voids, and (b) the void shape sensitivity parameter $\Delta E^{(c)}$ as a function of triaxiality T.

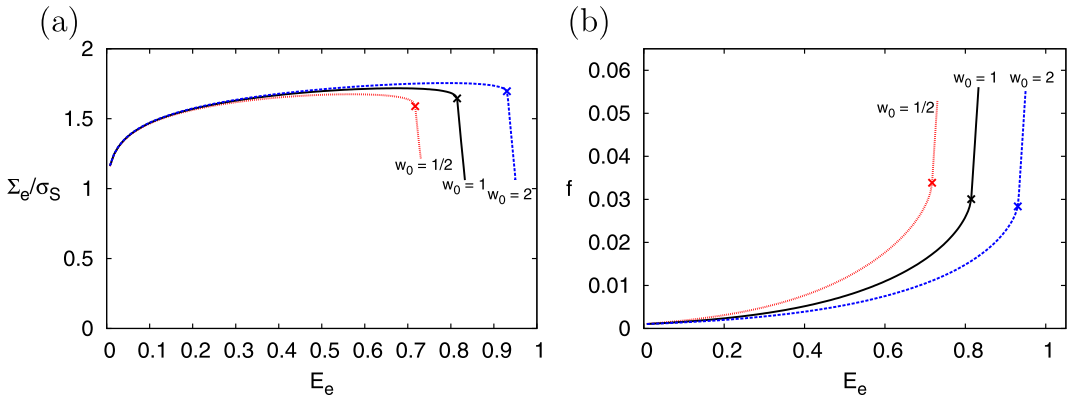

Fig. 8. Effect of initial void aspect ratio on the effective response of porous unit cells for an isotropic matrix, $f_0 = 0.001$, $\lambda_0 = 1$ and $T = 1$: (a) effective stress–strain response, (b) evolution of porosity.

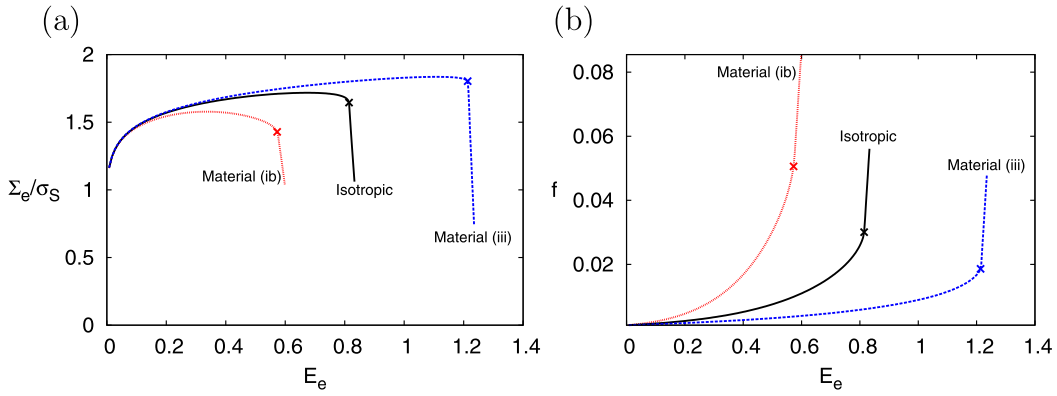

Fig. 9. Effect of matrix plastic anisotropy on the effective response of porous unit cells for EYT materials and spherical voids with $f_0 = 0.001$, $\lambda_0 = 1$ and $T = 1$: (a) effective stress–strain response, and (b) evolution of porosity.

conditions are identical to those previously analyzed by Benzerga and Besson (2001) except that the present calculations were pursued beyond the onset of void coalescence. Just like at high triaxialities, material anisotropy significantly affects both the flow stress and the strains to coalescence. Comparison of the two sets of results above shows that, in an isotropic matrix, the effective strains to coalescence range from 0.7 to 0.9 for initially oblate and prolate voids, respectively, (Fig. 8) while the range is from 0.6 to 1.2 for the three anisotropic materials considered in Fig. 9. This indicates that at moderate triaxialities both void shape effects and material anisotropy can significantly influence the material response.

In the above analyses, either the initial void shape or the matrix was isotropic. Interestingly, analysis of the combined effect of void shape and material anisotropy at $T = 1$ yields the results depicted in Fig. 10. Four sets of curves are shown which correspond to the cases of initially prolate ($w_0 = 2$) and oblate ($w_0 = 1/2$) voids in unit cells made of EYT materials (ib) and (iii). In the case of material (ib), material anisotropy appears to enhance the effect of initial void shape, while the effect of void shape is completely masked in the case of material (iii) (at least in the range of void shapes considered here). This result is not intuitive from inspection of the individual effects of void shape and material anisotropy in Figs. 8

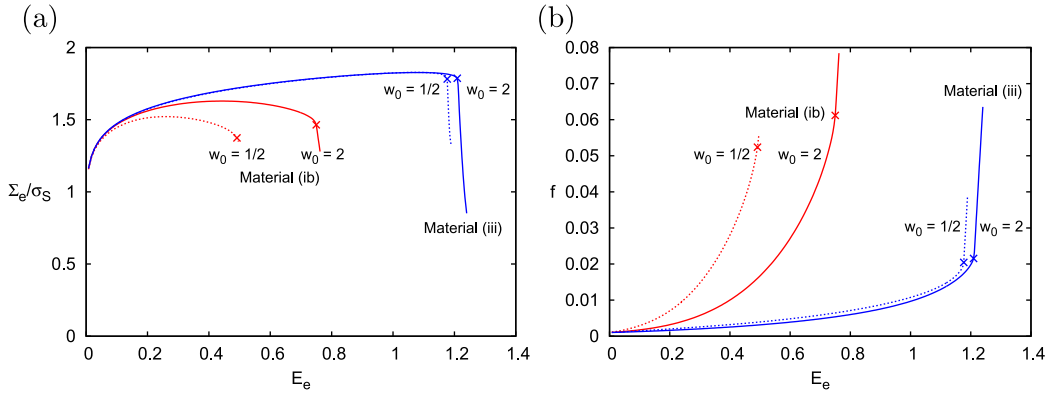

Fig. 10. Combined effect of void shape and matrix plastic anisotropy on the effective response of porous unit cells for EYT materials with $f_0 = 0.001$, $\lambda_0 = 1$, $T = 1$ and two values of the void aspect ratio: (a) effective stress–strain response, and (b) evolution of porosity.

and 9, respectively, and indicates a non-trivial coupling between the two. This effect is obviously not restricted to the particular conditions chosen here. A similar trend was reported in Fig. 7b for a much lower initial porosity $f_0 = 0.0001$.

In order to further illustrate the subtle coupling between void shape and plastic anisotropy, we examined contours of effective plastic strain in the matrix at a unit cell effective strain $E_e = 0.5$ for initially prolate voids ($w_0 = 2$) in all three EYT materials, Fig. 11. Conclusions from previous investigations of void shape effects (Pardoen and Hutchinson, 2000) had indicated that materials with more elongated voids consistently show higher ductility (slower growth of porosity with effective strain). However, further investigation reveals that the evolution of the void aspect ratio for the three unit cells in Fig. 11 (not shown) is roughly similar up to $E_e = 0.5$, as can be seen from the void shapes in Fig. 11. Despite this fact, material (ib) shows greater void growth than the isotropic matrix while material (iii) shows the least void growth at equal macroscopic strain levels. Also, the distribution of plastic strains in the matrix is different for the three materials with material (ib) showing a greater tendency for shear localization along an inclined band, due to its lower yield stresses in shear compared to the other materials.

In materials with enhanced shear-resistance (category (iii)), the effect of initial void shape is found to be negligible within the range $w_0 = 1/2$ to 2 (see Fig. 10 above). We have conducted additional calculations to explore a broader range of void shapes from $w_0 = 1/6$ to 6. The corresponding results are shown in Fig. 12 for two values of the initial porosity. The results show that the strains to coalescence $E^{(c)}$ are not significantly changed for larger values of w_0 (>2), while flatter voids ($w_0 = 1/6$) lead to a reduction in ductility, although not to the extent expected for isotropic materials.

Next, for the same category of materials (iii) with enhanced shear resistance, we examine the conditions on the anisotropy parameters that lead to the non-trivial coupling between void

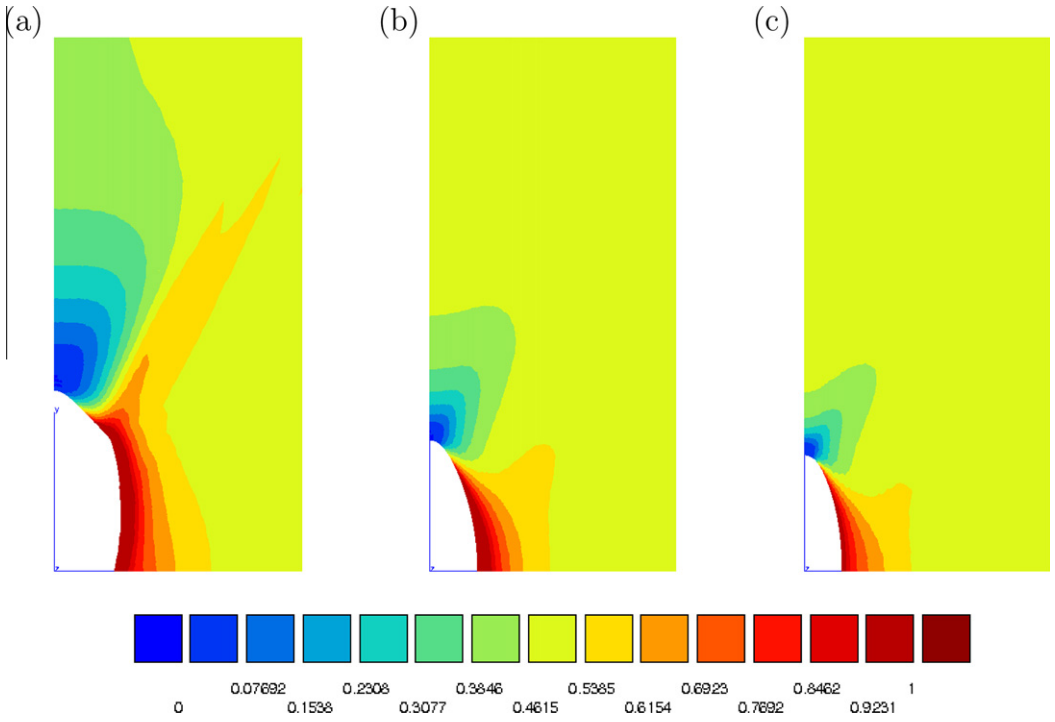

Fig. 11. Contours of effective plastic strain p at $E_e = 0.5$ for initially prolate voids with $f = 0.001$, $w_0 = 2$ and $T = 1$: (a) material (ib), (b) isotropic matrix, and (c) material (iii).

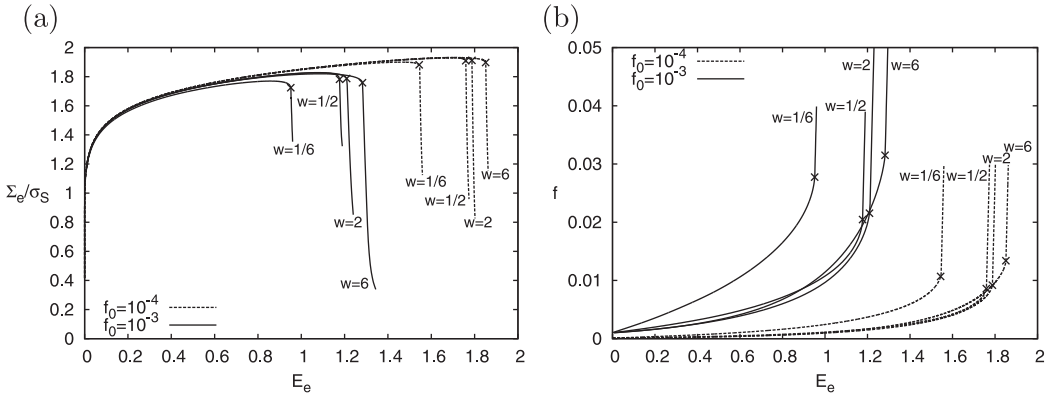

Fig. 12. An elaboration on the results of Fig. 10 for material (iii) over a wider window of initial void aspect ratios w_0 for two values of initial porosity, $\lambda_0 = 1$ and $T = 1$: (a) effective stress–strain response, and (b) evolution of porosity.

shape and matrix flow anisotropy. The difference between an isotropic matrix and material (iii) lies in the values of the shear Hill coefficients, with $h_{TS} = h_{SL} = 0.5$ for material (iii) as opposed to unity for the isotropic material (see Table 1). In Fig. 13, we continuously vary the values of h_{TS} between 0.25 and 1 to observe the effect on the void shape sensitivity for the coalescence strains and the growth rate of porosity. Two values of initial void shapes, $w_0 = 1$ and $w_0 = 1/2$, are compared. One can see that a transition occurs approximately at $h_{TS} = 0.5$ below which the difference between the curves corresponding to the two initial void shapes is negligible. Fig. 14 shows the variation of the void shape sensitivity parameter $\Delta E^{(c)}$, defined in Eq. (13), as a function of the Hill coefficients h_{TS}. The void shape sensitivity is seen to increase with increasing h_{TS} with an inflexion point around the isotropic value of $h_{TS} = 1$. The void shape sensitivity approaches zero for $h_{TS} < 0.5$ (materials of type (iii)) whereas the void shape sensitivity is seen to be high for $h_{TS} > 2$ (materials of type (i)).

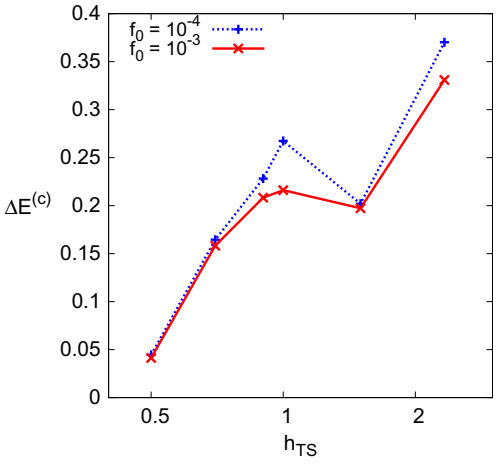

Fig. 14. Variation of the void shape sensitivity parameter $\Delta E^{(c)}$ for a wide range of EYT materials described by the out-of-plane shear Hill coefficient h_{TS}. Matrix materials with $h_{TS} < 1$ are shear-resistance (type (iii)) and matrices with $h_{TS} > 1$ are weak in shear (type (i)).

3.4. Case of penny shaped cracks

The limiting case of highly oblate voids or penny shaped cracks is an important one in practice. Such cracks were observed to initiate in brittle phases in multi-phase materials (Pineau and Joly, 1991; Bugat et al., 2001) or simply due to cracking of second phase particles; see the review by Benzerga and Leblond (2010). Lassance et al. (2006) carried out a series of cell model studies of penny shaped voids embedded in an isotropic matrix. In this section, we explore amendments to their conclusions when matrix anisotropy is taken into account. Attention is restricted to the same EYT materials investigated above. One issue with using the cell model of Fig. 1 for particle–matrix systems is that it ignores the effect of particles. A useful result in this respect from Lassance et al.'s (2006) investigation is that particle shielding is weak for particle volume fractions below 1% or so. We shall rely on this finding to justify the relevance of the voided cell model to particle–matrix material systems, in addition to multi-phase ones.

Three realizations of the penny-shaped crack were investigated using $w_0 = 1/30$, $w_0 = 1/20$ and $w_0 = 1/10$ keeping the same radial void size to void spacing ratio ($\chi_0 = 0.247$). Such initial configurations correspond to different values of the initial porosity but share the same value of the equivalent porosity $f_0^e = 0.01$. Here, f_0^e is defined as the volume fraction of a spherical void having a radius equal to that of the "crack". The actual porosity $f_0 = w_0 f_0^e$ is therefore much smaller. It was found that the response of the unit cell is weakly dependent upon the specific choice of w_0 in the range considered, irrespective of the type of material anisotropy. Thus, we will only present results for $w_0 = 1/20$ focussing on the effect of matrix anisotropy.

Fig. 15 shows the results obtained for a loading triaxiality of $T = 1$ (solid lines). These results clearly indicate that the effect of matrix anisotropy is as significant in this limit case of penny shaped cracks as it is for other void shapes. For instance the effective strain to coalescence for material (iii) is about twice as much as for material (ib). This effect was qualitatively expected because the crack quickly blunts in the matrix and opens up into a void with a roughly equiaxed shape.

To interpret further these results, a set of reference calculations were carried out for the equivalent microstructure, i.e., for spherical voids with $f_0 = 0.01 = f_0^e$. The corresponding results are also included in Fig. 15 (dashed lines). An interesting finding in the case of material (iii) is that the response for penny shaped cracks is very different from that obtained for the equivalent spherical voids. This puts into question the very notion of "equivalence". On the other hand, it is noted that the responses for the equivalent and actual microstructures are indeed close to each other in the case of the isotropic matrix and material (ib). It is possible to explain why this equivalence works well for isotropic matrices. In fact, it results from the competing effects of extremely oblate shape (negative for ductility) and low initial porosity (positive). When the two effects cancel out "equivalence" works. However, deviations from that behavior are conceivable in the presence of large deformation

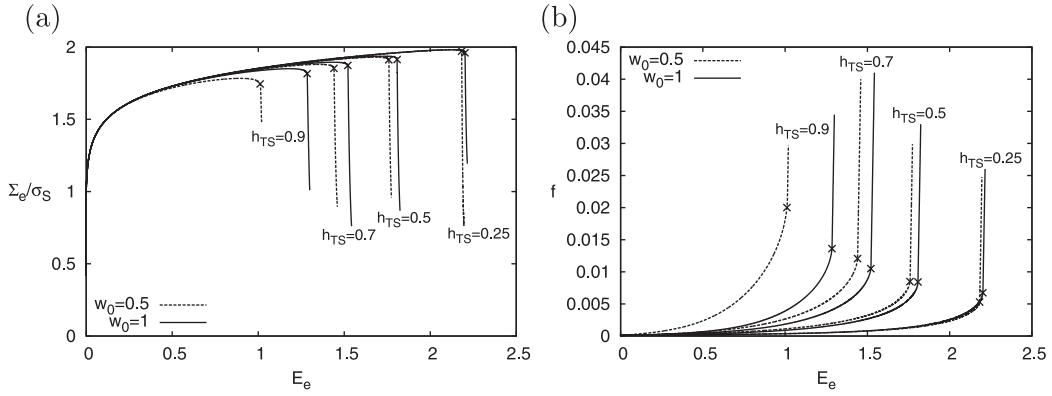

Fig. 13. Transition from a material (i) type behavior to a material (iii) type behavior. Effect of varying the out-of-plane "shear" Hill coefficient, h_{TS}, on the effective response of porous unit cells with $f_0 = 0.001$, $\lambda_0 = 1$ and $T = 1$: (a) effective stress–strain response, and (b) evolution of porosity.

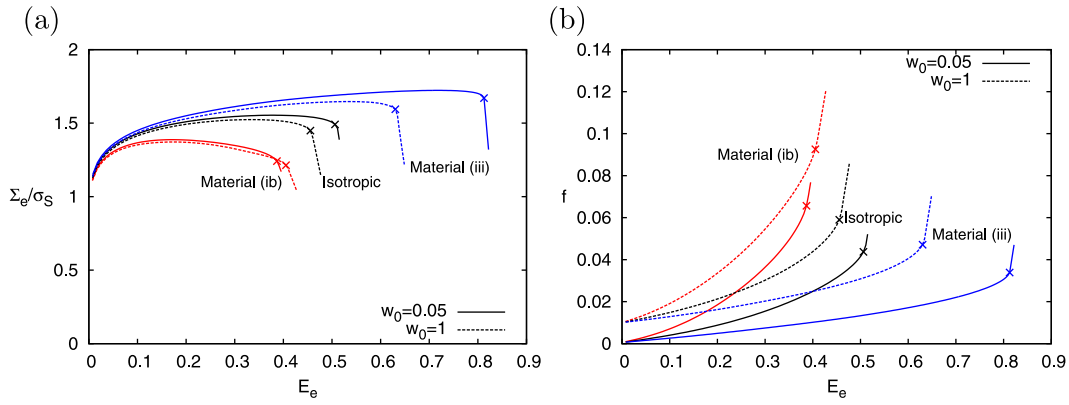

Fig. 15. Effect of matrix plastic anisotropy on the effective response of porous unit cells containing initially penny shaped cracks ($w_0 = 1/20$) with and effective porosity $f_0^s = 0.01$ (solid lines) and spherical voids with $f_0 = 0.01$ (dashed lines), under axisymmetric loading with $T = 1$: (a) effective stress–strain response, and (b) evolution of porosity.

induced microstructure evolution. Such deviations are realized in materials of type (iii) as shown in Fig. 15.

3.5. Materials with unequal principal yield strengths

The material anisotropy parameters used in the set of results presented thus far were chosen such that the materials have the same nominal yield stresses in the three principal directions of orthotropy ($h_L = h_T = h_S = 1$). As a consequence, for all such EYT materials the unit cell effective and mean normal stresses are initially equal. Since the evolution of porosity has an exponential dependence on the mean stress, the choice of EYT materials enabled us to apportion the effects of material anisotropy and void shape. However, the case of h_L, h_T, $h_S \neq 1$ is more general and commonly observed experimentally (Benzerga et al., 2004a). In this section, we present a set of results for categories of materials with $h_L = h_T \neq 1$ and $h_S \neq 1$.

Fig. 16a shows the comparison of stress–strain responses for unit cells made of an isotropic matrix, material (iib) and material (iv) from Table 1. Material (iib) is similar to material (ib) from the previous set of calculations in the sense that they both have relatively high values of the shear Hill coefficients $h_{TS}(=h_{SL})$ compared to the isotropic case making them weaker under shear loading. On the other hand, material (iv) is weaker under tension along the principal directions similar to material (iii) used previously. Three different values of w_0 (=1/2, 1 and 2) are compared and all the unit cells had $f_0 = 0.001$ and $\lambda_0 = 1$. Each of these materials has the same yield strengths $\sigma_L = \sigma_T$ in the radial direction but

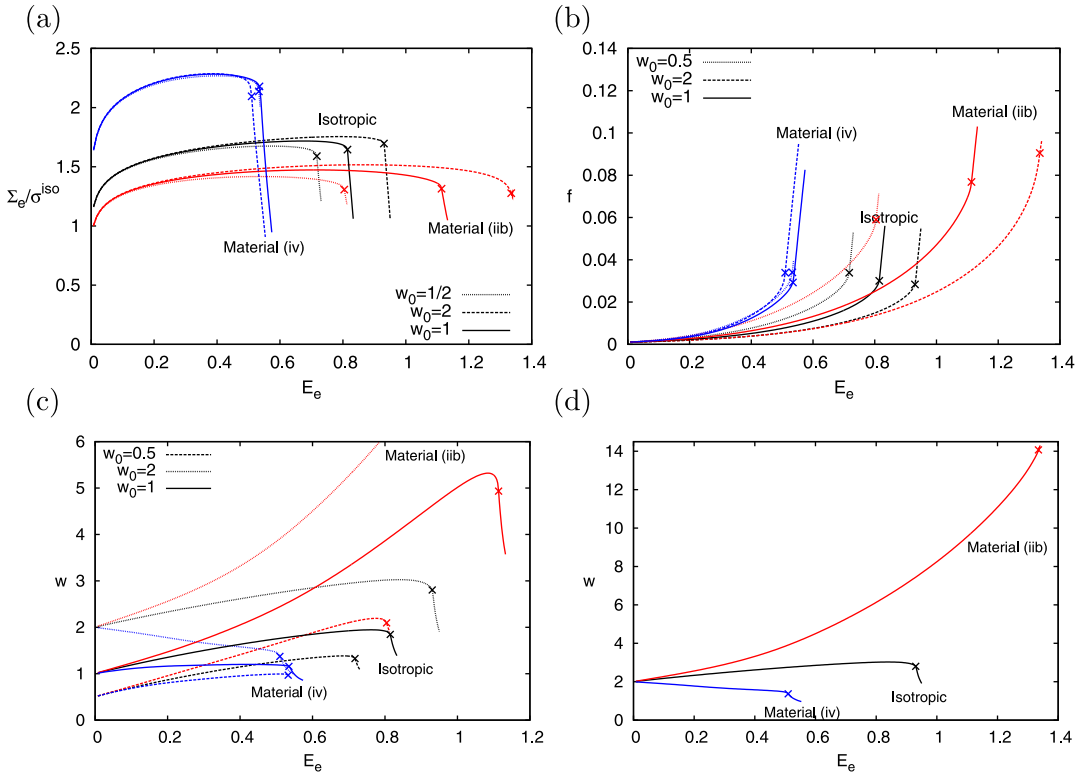

Fig. 16. Effect of matrix material anisotropy on the cell model response for $f_0 = 0.001$, $\lambda_0 = 1$, $T = 1$ and three values of w_0. Case of non EYT materials (Table 1). (a) Effective stress–strain response, (b) evolution of porosity, (c) evolution of the void aspect ratio w; and (d) evolution of w for initially prolate cavities with $w_0 = 2$. The anisotropic materials being compared have different yield stresses in uniaxial tension along $\mathbf{e}_S$.

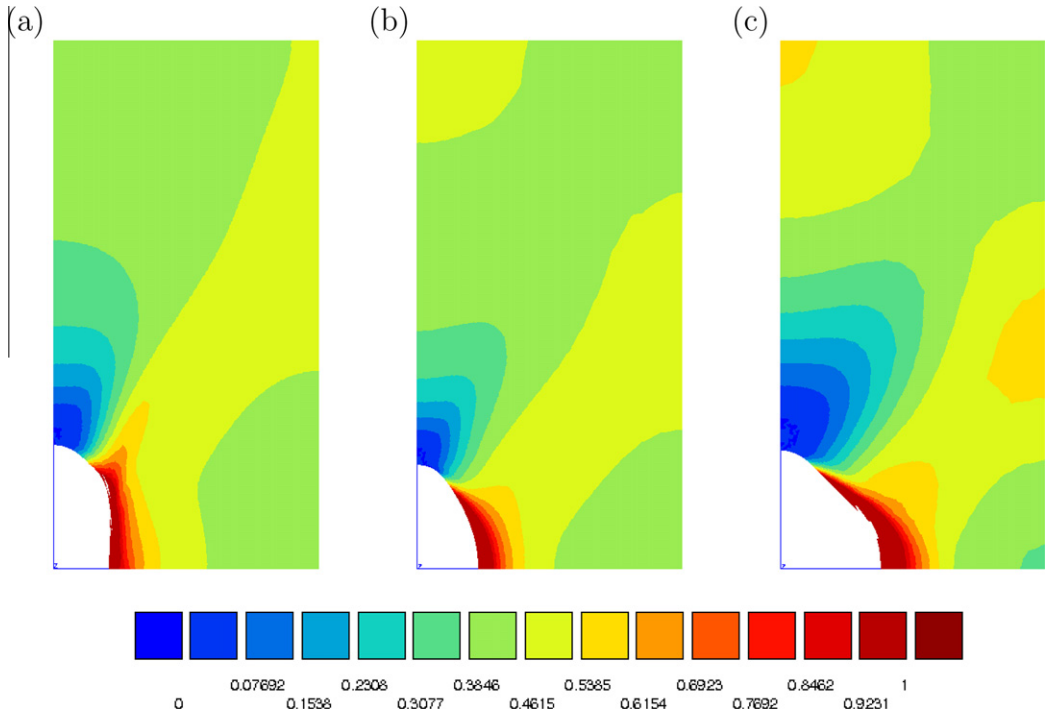

Fig. 17. Contours of effective plastic strain p at $E_e = 0.45$ for non EYT materials and initially spherical voids with $f = 0.001$ and $T = 1$: (a) material (iib), (b) isotropic matrix, and (c) material (iv).

the axial yield strength σ_S varies for each material. For comparison purposes, the effective stresses in Fig. 16a are normalized by the initial yield stress, σ^{iso}, of the isotropic matrix. This avoids normalization by a variable quantity.

One can see from Fig. 16a that material (iv) has the highest effective strength while material (iib) has the lowest strength. Clearly, the effect of the overall stress level reflects in the evolution of the porosity shown in Fig. 16b, where material (iv) consistently shows faster void growth compared to material (iib). Nevertheless, some qualitative features of the effect of the shear Hill coefficients $h_{TS} = h_{SL}$ observed in the previous calculations are retained. For instance, the effect of the initial void shape is seen to be negligible for material (iv) while the effect is magnified for material (iib) (in comparison to the case of the isotropic matrix). These trends are identical to those observed for material (iii) and material (ib), respectively, in the previous sections. One common feature of these results is that orthotropic materials that are weaker under shear in one of their principal planes compared to an isotropic material (i.e. $h_{TS} = h_{SL} > 1$ in the transverse isotropic case) appears to exhibit higher sensitivity to the initial void shape, while materials that have a high resistance to yielding under shear exhibit lower void shape sensitivity.

Fig. 16c shows the evolution of the void aspect ratio w and Fig. 16d shows the evolution of w in the $w_0 = 2$ case with an expanded range for the ordinate. The interesting observation from Fig. 16d is that the mode of coalescence in the case of material (iib) appears to be different from the case of the other materials. Although the cell exhibits a transition to the uniaxial straining mode, this is not accompanied by a corresponding drop in w associated with the rapid lateral expansion of the voids. In fact, examination of the contours of effective plastic strain in the deformed configuration of the unit cell (Fig. 17) reveals that significant plastic strain has accumulated along an inclined band in the case of material (iib). This eventually leads to significant deviations from a spheroidal shape for the cavity. As a result, coalescence takes place in a plane parallel to the equatorial plane, by necking of the smallest deformed ligament. A more thorough investigation of the conditions under which these alternate modes of coalescence are favored under axisymmetric loading will be provided in a forthcoming companion paper.

4. Discussion

The primary motivation for pursuing cell model studies of the type presented in this paper is to analyze the influence of matrix material anisotropy on void growth and coalescence. Previous finite element cell studies have focussed on the separate effects of void shape (Sovik and Thaulow, 1997; Pardoen and Hutchinson, 2000; Gao and Kim, 2006) and plastic flow anisotropy in single crystals (Yerra et al., 2010) or textured polycrystals (Benzerga and Besson, 2001). The aim of this paper has been to assess the relative importance of void shape and plastic anisotropy effects on ductile fracture under a variety of triaxial proportional loading conditions. The results of the present study also provide benchmarks for calibrating continuum models of ductile fracture in anisotropic materials. These include extensions of the Gurson model to incorporate additional microstructural information, such as void shape and material texture (Gologanu et al., 1997; Benzerga and Besson, 2001; Monchiet et al., 2008; Keralavarma and Benzerga, 2008; Keralavarma and Benzerga, 2010), as well as alternative porous metal plasticity models accounting for texture effects in polycrystalline materials (Lebensohn et al., 2004). Furthermore, once appropriately extended to account for plastic anisotropy, the void coalescence models that were independently developed by Gologanu et al. (2001), Pardoen and Hutchinson (2000) and Benzerga (2002) can also be assessed using the present findings from cell model calculations.

The voided cell model is a powerful tool for investigating ductile failure mechanisms at intermediate scales. Three kinds of parameters enter the model, which relate to the applied loading, the microstructure (i.e., void population attributes) and the plastic

flow in the matrix. When the present results are added to the rich literature on this subject (Benzerga and Leblond, 2010), it becomes evident that the effect of matrix anisotropy is most important among all matrix related parameters, including strain hardening. To illustrate this, the $E^{(c)}$ measure of failure strain decreases by more than 0.7 when Hill coefficient h_{TS} varies between 0.5 and 2.33 for an initial porosity of $f_0 = 0.001$. For reference, the relative change in failure strain is about 0.7 for the same f_0 when the stress triaxiality ratio varies between 1 and 3. The effect of matrix anisotropy is thus comparable to the exponential effect of triaxiality.

To understand the effect of matrix anisotropy, consider the following combination of Hill's coefficients

$$h = 2\left[\frac{2}{5}\frac{h_L + h_T + h_S}{h_L h_T + h_T h_S + h_S h_L} + \frac{1}{5}\left(\frac{1}{h_{TS}} + \frac{1}{h_{SL}} + \frac{1}{h_{LT}}\right)\right]^{\frac{1}{2}}. \tag{14}$$

For an isotropic material $h = 2$. This scalar is an invariant of the fourth order tensor $\mathbb{h}$, expressed in axes pointing toward the principal directions of matrix orthotropy. It has emerged in all previous analytical treatments of the problem at hand, or variants thereof, by means of homogenization theory (Benzerga and Besson, 2001; Monchiet et al., 2008; Keralavarma and Benzerga, 2010). According to these theoretical models, the growth rate of porosity may be written as

$$\dot{f} \propto \sinh\left(\kappa \frac{\Sigma_h}{\bar{\sigma}}\right), \tag{15}$$

where Σ_h is a weighted mean of the normal stresses, $\bar{\sigma}$ is the matrix flow stress and κ is a factor that depends on both void shape and matrix anisotropy. Interestingly, κ has a $1/h$ dependence and is exactly $3/h$ for spherical voids. The essence of the effect of matrix anisotropy on void growth is rooted in the way invariant h changes from one material category to another. The values taken by h, as reported in Table 1, correlate with the trends observed for all materials investigated. In particular, the exponential dependence of void growth upon stress triaxiality (through Σ_h) and matrix anisotropy (through h) clarifies the comparable effects of T and anisotropy pointed out above. Yerra et al. (2010) have also pointed out the usefulness of Eq. (14) as a rationale for their results on void growth in single crystals.

Our results show that the effect of matrix anisotropy is both persistent and subtle. The persistent effect, including at extreme stress triaxialities or void shapes, is essentially explained by an average resistance to void growth represented by invariant h. On the other hand, the effect can be subtle due to varying stress levels (such as in materials with unequal yield strengths) or to strong coupling with void shape effects. In fact, the factor κ in (15) may depend on other transversely isotropic invariants of tensor $\mathbb{h}$, as inferred from the theoretical analysis of Keralavarma and Benzerga (2010). Such subtleties may also explain some trends discussed by Yerra et al. (2010).

We emphasize that the average resistance introduced through h arises irrespective of the major load direction. Evidently, some additional dependence upon load direction will manifest in any anisotropic material. The analysis of any such dependence would require fully 3D calculations. The key finding is that any given material is characterized by a factor h, which sets its average resistance to void growth.

Among the obtained trends some findings merit further discussion. At high levels of remote load triaxiality ($T \geqslant 2$), the effect of material plastic anisotropy is a predominant factor affecting the overall ductility, unlike the effect of void shape (Figs. 4–6). A continuum model for plastically orthotropic porous materials has previously been developed by Benzerga and Besson (2001) following a micromechanics based approach similar to that of Gurson (1977). It was demonstrated that this model captured well the effect of material anisotropy on the effective response of the porous medium, as evidenced by comparisons of the model with unit cell calculations of the type presented here using initially spherical voids. Since at high T, void shape evolution has a negligible effect for initially spherical cavities, the model of Benzerga and Besson (2001) neglecting void shape effects is an adequate extension of the Gurson model to plastically anisotropic materials.

The behavior at moderate stress triaxialities ($2/3 \leqslant T \leqslant 1.5$) prevailing in notched bars can be quite different. As is now widely documented in the literature, void shape effects are important in this regime. This effect is best quantified using a void shape sensitivity parameter, ΔE^c, defined as the difference between strains to coalescence for initially prolate and oblate voids.[1] At high triaxiality, $\Delta E^{(c)} \approx 0$ whereas at $T = 1$ the difference in ductilities is already above 0.25. This figure increases further upon decreasing the triaxiality down to $T > 1/3$. For $T = 1/3$, void coalescence does not take place for $f_0 \leqslant 0.001$, irrespective of the initial void shape (Pardoen and Hutchinson, 2000). In the regime of moderate triaxialities, the cell model studies reported on here show that the sensitivity to initial void shape is influenced by matrix material anisotropy. This influence is so strong that it may either nullify the effect of void shape (e.g. material (iii) in Fig. 10) or exacerbate it, as is the case of materials (ib) and (iib) in Figs. 10 and 16, respectively. Typical trends can be summarized using the above notion of void shape sensitivity parameter $\Delta E^{(c)}$, as shown in Fig. 7b. In this regard, Benzerga et al. (2004b) used a heuristic combination of the models by Benzerga and Besson (2001) and Gologanu et al. (1997) in their modeling of anisotropic fracture. For weak coupling between void shape and matrix anisotropy effects, their heuristic combination is acceptable but the present results indicate the extent to which such heuristics is valid.

This study does not deal with the conditions under which voids nucleate in real materials. Any predictions made on the basis of the results reported here would need to be augmented with detailed nucleation analyses. Yet, voids are reported to nucleate at rather low macroscopic strain levels in various material systems (e.g., sulfides in steels and cracks in brittle phases). In addition, when void nucleation occurs due to brittle particle cracking, penny-shaped cracks form and blunt into the plastically flowing matrix.

Our findings for penny-shaped voids confirm that the influence of plastic anisotropy in ductile fracture is paramount. This was illustrated for EYT materials at a moderate triaxiality of 1 and the same behavior is expected at higher triaxialities which promote faster evolution of voids into equiaxed shapes. For all EYT materials that were considered, the cell model response was found to be independent of the specific choice of the "crack" aspect ratio so long as $w_0 \leqslant 1/10$. This is in agreement with the conclusions of Lassance et al. (2006) who studied the case of isotropic matrices. As noted there, the ductility of isotropic materials containing penny-shaped cracks is controlled by the relative void spacing. Since the latter was kept fixed in our investigation, we conclude that matrix anisotropy is another important microstructural parameter along with the relative void spacing. With respect to approximating penny-shaped cracks with equivalent spherical voids, our findings for some materials support the proposition made long ago by Pineau and Joly (1991) who introduced the notion of an equivalent porosity f_0^e. Lassance et al. (2006) established one limitation of such an approximation, namely the case of large particle/void volume fractions. The present investigation establishes another limit for materials endowed with a higher resistance in shear than their isotropic counterpart (Fig. 15). This limitation of the equivalent microstructure applies at all porosity levels.

[1] The values chosen in the text for w_0, i.e., 1/2 and 2, are arbitrary. However, ΔE^c can be defined more objectively as the difference between infinitely long voids (cylinders) and infinitely flat voids (penny-shaped cracks).

Part of the effect of plastic anisotropy is associated with void growth. The other part can be associated with the way in which anisotropy affects the shift to the uniaxial straining mode, i.e., the onset and progress of void coalescence. It is not straightforward to apportion the two contributions from the cell model calculations alone. In the absence of an analytical quantitative model of void coalescence in anisotropic materials, one can document the values of the void volume fraction at incipient coalescence, i.e., at the onset of micro-scale localization. Fig. 18 illustrates the trends in terms of this "critical" porosity, designated $f^{(c)}$, versus stress triaxiality for three EYT materials. In all the cases shown, void coalescence took place by internal necking of the inter-void ligament. Fig. 18 illustrates that $f^{(c)}$ is significantly affected by the plastic anisotropy of the material and may vary as a function of the loading triaxiality even for an isotropic material. This finding emphasizes a point already made in the literature, e.g., (Benzerga et al., 1999; Pardoen and Hutchinson, 2000; Gao and Kim, 2006), that the use of a constant $f^{(c)}$ in the phenomenological approach to void coalescence is, in general, not adequate. At the rates of void growth preceding localization, a difference of half a percent in $f^{(c)}$ can lead to significant variations in the strain to coalescence $E^{(c)}$. What is important in Fig. 18 is that plastic anisotropy can lead to variations in $f^{(c)}$ that are stronger than those caused by the triaxiality alone. Capturing these effects requires micromechanics based models of void coalescence that take into account the cumulative effect of the deformation history in determining the critical conditions for the onset of coalescence.

The computations presented here were limited to transversely isotropic materials. Experimentally measured material anisotropies can be more general, and therefore the material properties used in this study are approximate axisymmetric representations of the range of material anisotropies observed experimentally. Yet, the effects of material anisotropy evidenced in this work are quite prominent. This suggests that even stronger effects may be expected in more realistic cases. The analysis of the latter would however require fully three-dimensional calculations. What is of particular practical importance is that plastic anisotropy effects are significant, unavoidable (e.g., due to processing) and sometimes beneficial. As such, they may prompt material designers to engineer anisotropy of certain types instead of limiting it. With this prospect in mind, this and other concurrent modeling efforts may help lay the theoretical foundations for such rational material design.

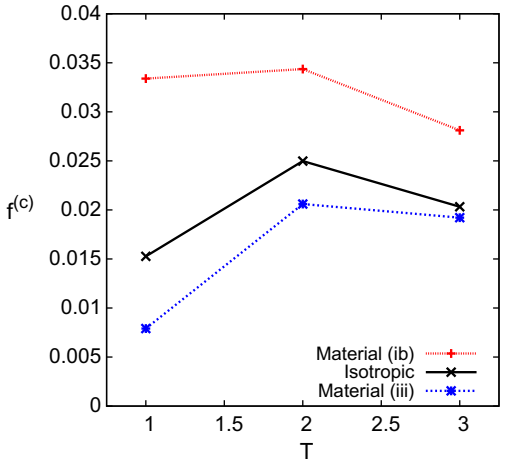

Fig. 18. Porosity at the onset of coalescence, $f^{(c)}$, versus stress triaxiality ratio, T, for initially spherical voids with $f_0 = 0.0001$ and three EYT matrix materials.

5. Conclusions

The effect of matrix material anisotropy on void growth and coalescence was investigated under a variety of axisymmetric loading conditions and for various initial microstructures representative of periodic void aggregates. The plastic anisotropy modeled here is a representation of material texture and grain elongation effects in polycrystalline materials. It can also represent the anisotropy of plastic flow in single crystals. The conclusions drawn from our results may be summarized as follows:

- The effect of plastic anisotropy of the matrix material appears to be a dominant factor in the mechanics of porous plastic solids, at all stress triaxiality levels. Unlike the effect of void shape, its effect does not vanish at high levels of triaxiality. In addition, at low stress triaxiality, plastic anisotropy sets the extent to which the initial void shape affects the effective behavior of the porous material.
- The critical porosity for the onset of coalescence $f^{(c)}$, which generally depends on the stress triaxiality ratio, is found to depend strongly on the plastic anisotropy of the matrix.
- Since void growth and coalescence are but expressions of plastic distortion of the matrix material, the above effects of plastic anisotropy are qualitatively expected. However, the magnitude manifested by these effects is far more significant than has been appreciated in the literature.
- The computational results clearly illustrate the need for a fundamental coupling between plastic anisotropy and void shape effects for accurate modeling of ductile fracture in structural materials. In this context, there is a need for better experimental characterization of the plastic flow anisotropy of wrought structural materials under fully three-dimensional conditions.

Acknowledgments

The authors acknowledge support from the National Science Foundation under grants DMR-0851828 and CMMI-0748187.

References

Barsoum, I., Faleskog, J., 2007. Rupture mechanisms in combined tension and shearG-Micromechanics. Int. J. Solids Structures 44, 5481–5498.
Benzerga, A.A., 2000. Rupture ductile des tôles anisotropes. Ph.D. Thesis, Ecole Nationale Supérieure des Mines de Paris.
Benzerga, A.A., 2002. Micromechanics of coalescence in ductile fracture. J. Mech. Phys. Solids 50, 1331–1362.
Benzerga, A.A., Besson, J., 2001. Plastic potentials for anisotropic porous solids. Eur. J. Mech. 20 (3), 397–434.
Benzerga, A.A., Besson, J., Pineau, A., 1999. Coalescence-controlled anisotropic ductile fracture. J. Eng. Mat. Tech. 121, 221–229.
Benzerga, A.A., Besson, J., Pineau, A., 2004a. Anisotropic ductile fracture. Part I: experiments. Acta Mater. 52, 4623–4638.
Benzerga, A.A., Besson, J., Pineau, A., 2004b. Anisotropic ductile fracture. Part II: theory. Acta Mater. 52, 4639–4650.
Benzerga, A.A., Leblond, J.B., 2010. Ductile fracture by void growth to coalescence. Adv. Appl. Mech. 44, 169–305.
Besson, J., Foerch, R., 1997. Large scale object oriented finite element code design. Comput. Methods Appl. Mech. Eng. 142, 165–187.
Bugat, S., Besson, J., Gourgues, A.F., Pineau, A., 2001. Microstructure and damage initiation in duplex stainless steels. Mater. Sci. Eng. 317, 32–36.
Gao, X., Kim, J., 2006. Modeling of ductile fracture: Significance of void coalescence. Int. J. Solids Struct. 43, 6277–6293.
Gologanu, M., Leblond, J.-B., Devaux, J., 1993. Approximate models for ductile metals containing non-spherical voids – case of axisymmetric prolate ellipsoidal cavities. J. Mech. Phys. Solids 41 (11), 1723–1754.
Gologanu, M., Leblond, J.-B., Perrin, G., Devaux, J., 1997. Recent extensions of Gurson's model for porous ductile metals. In: Suquet, P. (Ed.), Continuum Micromechanics, CISM Lectures Series. Springer, New York, pp. 61–130.
Gologanu, M., Leblond, J.-B., Perrin, G., Devaux, J., 2001. Theoretical models for void coalescence in porous ductile solids – I: coalescence in "layers". Int. J. Solids Struct. 38, 5581–5594.

Gurson, A.L., 1977. Continuum theory of ductile rupture by void nucleation and growth: Part I– yield criteria and flow rules for porous ductile media. J. Eng. Mat. Tech. 99, 2–15.

Hill, R., 1948. A theory of yielding and plastic flow of anisotropic solids. Proc. Roy. Soc. London A 193, 281–297.

Hom, C.L., McMeeking, R.M., 1989. Void growth in elastic–plastic materials. J. Appl. Mech. 56, 309–317.

Hughes, T., Winget, J., 1980. Finite rotation effects in numerical integration of rate constitutive equations arising in large-deformation analysis. Int. J. Numer. Methods Eng. 15, 1862–1867.

Keralavarma, S.M., Benzerga, A.A., 2008. An approximate yield criterion for anisotropic porous media. C.R. Mecanique 336, 685–692.

Keralavarma, S.M., Benzerga, A.A., 2010. A constitutive model for plastically anisotropic solids with non-spherical voids. J. Mech. Phys. Solids 58, 874–901.

Kim, J., Gao, X., Srivatsan, T., 2004. Modeling of void growth in ductile solids: effects of stress triaxiality and initial porosity. Eng. Fract. Mech. 71, 379–400.

Koplik, J., Needleman, A., 1988. Void growth and coalescence in porous plastic solids. Int. J. Solids Struct. 24 (8), 835–853.

Ladeveze, P., 1980. Sur la théorie de la plasticité en grandes déformations. Tech. Rep. 9. L.M.T. Ecole Normale Supérieure, Cachan, France.

Lassance, D., Scheyvaerts, F., Pardoen, T., 2006. Growth and coalescence of penny-shaped voids in metallic alloys. Eng. Fract. Mech. 73, 1009–1034.

Lebensohn, R., Tomé, C., Maudlin, P., 2004. A selfconsistent formulation for the prediction of the anisotropic behavior of viscoplastic polycrystals with voids. J. Mech. Phys. Solids 52, 249–278.

Monchiet, V., Cazacu, O., Charkaluk, E., Kondo, D., 2008. Macroscopic yield criteria for plastic anisotropic materials containing spheroidal voids. Int. J. Plast. 24, 1158–1189.

Needleman, A., 1972. A numerical study of necking in circular cylindrical bars. J. Mech. Phys. Solids 20, 111–127.

Pardoen, T., Hutchinson, J.W., 2000. An extended model for void growth and coalescence. J. Mech. Phys. Solids 48, 2467–2512.

Pineau, A., Joly, P., 1991. Local versus global approaches of elastic–plastic fracture mechanics. application to ferritic steels and a cast duplex stainless steel. In: Blauel, J., Schwalbe, K. (Eds.), Defect Assessment in Components – Fundamentals and Applications. ESIS, European Group on Fracture Publication, pp. 381–414.

Simo, J.C., Taylor, R.L., 1985. Consistent tangent operators for rate independent elasto-plasticity. Comput. Methods Appl. Mech. Eng. 48, 101–118.

Sovik, O., Thaulow, C., 1997. Growth of spheroidal voids in elastic–plastic solids. Fatigue Fract. Eng. Mater. Struct. 20, 1731–1744.

Tvergaard, V., 1982. On localization in ductile materials containing spherical voids. Int. J. Fract. 18, 237–252.

Tvergaard, V., Needleman, A., 1984. Analysis of the cup–cone fracture in a round tensile bar. Acta metall. 32, 157–169.

Worswick, M.J., Pick, R.J., 1990. Void growth and constitutive softening in a periodically voided solid. J. Mech. Phys. Solids 38 (5), 601–625.

Yerra, S., Tekoglu, C., Scheyvaerts, F., Delannay, L., Houtte, P.V., Pardoen, T., 2010. Void growth and coalescence in single crystals. Int. J. Solids Struct. 47, 1016–1029.

Zhang, K.S., Bai, J.B., Francois, D., 2001. Numerical analysis of the influence of the Lode parameter on void growth. Int. J. Solids Struct. 38, 5847–5856.